IEEE Access
Multidisciplinary ⋮ Rapid Review ⋮ Open Access Journal

Received 11 January 2023, accepted 18 February 2023, date of publication 24 February 2023, date of current version 1 March 2023.

Digital Object Identifier 10.1109/ACCESS.2023.3249111

RESEARCH ARTICLE

Control of PMSM Drive Using Lookup Table Based Compensated Duty Ratio Optimized Direct Torque Control (DTC)

BERHANU DEGGEFA LEMMA AND SRINIVASAN PRADABANE, (Member, IEEE)
Department of Electrical Engineering, National Institute of Technology Warangal, Warangal, Telangana 506004, India
Corresponding author: Berhanu Deggefa Lemma (bezakiyya@gmail.com)

ABSTRACT There are several ways to reduce the ripple magnitude for direct torque-controlled permanent magnet synchronous motor (PMSM) drives. In this work, the compensated duty ratio optimized direct torque control (DDTC-TC) method was proposed to reduce the ripple magnitude for three-phase PMSM. The proposed control strategy employs the simplicity of conventional DTC (CDTC) and compensation of the reference torque to enforce the developed torque to oscillate around the required value. A torque error square minimization technique was employed to determine the duty ratio. Magnitude of developed torque by the PMSM depends on the torque slope during the active and null voltage periods. The slope of the torque during each period is computed online. Based on the online computed slopes, the magnitude of the switching period and compensation torque were calculated. The ripple reduction capability of the proposed control scheme is tested using Matlab Simulink and a hardware in loop system. Both experimental and simulation results indicate that the control scheme is effective. Specifically, the torque and speed ripples are very small. The torque ripple during speed fluctuation is less for open-end winding PMSM. In addition, the proposed scheme was tested for four-quadrant operation. Results for four quadrants indicate that the scheme is effective for four quadrant operation. Finally, verification of the effectiveness of the proposed scheme is performed using OPAL-RT-RT (OP4500). Verification indicates that the proposed scheme is effective.

INDEX TERMS Compensation, DTC, harmonic, lookup table, OPAL-RT, optimization, PMSM, ripple.

I. INTRODUCTION

The performance of PMSM makes them universally accepted for various applications. Although PMSM has high efficiency, power density, and compact nature, it has a high ripple when a conventional DTC algorithm is used for controlling purposes. It is recommended to use DTC for drive applications that require rapid response time. PMSM provides a quick response in torque when the torque angle is rapidly manipulated by omitting the null voltage. Several studies have been conducted by different authors to reduce the drawbacks associated with DTC of PMSM drives. A predictive DTC with an optimized duty ratio is proposed for the PMSM drive to improve its performance. To reduce the error between required and motor responses, the motor parameter dependent prediction of current was forwarded in [1]. The optimum switching time coupled with predictive control (MP-DTC) minimizes the ripple.

The ripple and oscillation of the torque of PMSM originate from the nature of the distortion in the current. To enhance the performance of the PMSM drive controlled by DTC, the maximum torque per ampere (MTPA) based DTC was proposed in [2]. Improvement of active power loss in a motor winding has a significant impact on PMSM performance. In [3], a new PMSM model was presented for low-speed range electric drive applications. While an artificial intelligence approach was employed to optimize PMSM dynamics in [4]. In [5], the effect of one-step delay compensation on the voltage for predicting the next step current is addressed. By compensating for one step

The associate editor coordinating the review of this manuscript and approving it for publication was Hassan Omar.

delay in predicting the control signal and determining the optimum switching duration, torque ripple can be reduced.

Torque ripples and flux fluctuations can be reduced by using an extended finite vector (EFV-DTC) of three-six active state voltages by varying the duty [6]. Changes in both torque and flux at discrete duty cycles are recorded offline. The ripples are reduced by selecting a vector based on a trend. By using the torque and flux data from the offline trend, a balanced three-phase voltage is supplied to the motor. In [7], the issue of using a midpoint saturation controller (MPS-DTC) to obtain multiple voltages was discussed. This controller allows the output of multiple voltages. With an adaptive regulator, changing the duty ratio from zero to one can be achieved. The duty determination is made based on an error magnitude and a duty ratio for zero error. Instead of using fixed hysteresis control, saturation control can reduce the ripple. Relative to a nominal DTC, a saturation controller will improve the steady-state response.

In [8], ripple torque reduction was achieved with duty ratio determination, where the speed, error in flux, error in torque, and voltage vector were used to determine the duty ratio. Based on the similarity between the maximum ripple torque, the minimum switching duration, and the maximum switching period, the duty ratio can be calculated. To determine the duty ratio for DTC of PMSM based on torque error root square minimization (DDTC-TERSM) is employed in [9]. A comparison between DTC, model predictive-based direct torque control (MPDTC), and FOC was presented in [10]. Duty ratio optimized DTC (DDTC) performs better than CDTC. While MPDTC has superior performance in terms of torque ripple, current harmonics, and flux ripple. MPDTC has a simpler algorithm than DDTC, while DTC has a simpler algorithm. The concept of duty ratio optimized DTC with voltage phase angle compensation (DDTC-VAC) was proposed in [11]. For torque ripple reduction, duty ratio optimization is used, whereas voltage phase angle compensation is used for flux magnitude control. The torque error is used as an input to separate the ripple from the dynamics. For small torque errors, the flux and torque are forced to be equal to the required value. Alternatively, if the torque error is high, both the voltage and phase angle are set at levels that provide the best dynamic response.

In [2], the MTPA of current generation without the inclusion of quadrature axis currents was proposed for DTC of PMSM. This minimizes flux fluctuations due to saturation. For minimizing the torque and flux ripple for DTC, duty ratio determination using a rate of deviation of current was proposed in [12]. For current squared error minimization-based DTC (DDTC-CESM), the algorithm becomes complex when both d-q axis currents are considered separately. A simple method to get the duty ratio by only considering errors in torque and speed was proposed in [13]. If both axis inductances are equal, only the quadrature axis voltage is responsible for compensating for the change in torque and counter voltage. The computation burden for deadbeat causes difficulty in calculating the reference voltage when DTC-SVM is used for control of electric drive [14]. This difficulty is reduced by decoupling the equations for torque and flux. Optimized constant switching PWM-based DTC was forwarded to enhance the performance of the PMSM drive in [15]. The ripple level for both torque and flux are minimized by optimizing the on-time level of a selected voltage. According to this work, vector selection depends on the sign of torque deviation, flux, and flux angle.

The idea of torque ripple minimization using better flux estimation and adding the nullifying torque due to a fault current was proposed to reduce the ripple torque for PMSM drive systems under faulty conditions [16]. To include the torque deviation during the faulty condition, the magnitude of the torque due to fault current is added to the reference torque and compared with the actual torque. The switching of devices is done in the same manner as conventional DTC. A virtual torque reference manipulation for the reduction of ripple for DTC controlled PMSM drives is forwarded in [17]. A minimum voltage vector error-based DTC (DTC-MVVE) was applied to reduce ripple in [18]. For the n sector, Vn+1 is used to increase both, whereas to reduce the torque and increase the flux, Vn+5 is applied. The voltage Vn+2 is used to increase the torque and reduce the flux, whereas Vn+4 is used to reduce both, respectively. A nonlinear fuzzy system was employed for online control of the d-axis current to reduce the torque ripple [19]. The ripple reduction was performed by controlling the d-axis current only. In [20], current waveform optimization was employed along with the MTPA algorithm for ripple minimization.

In this work, a duty ratio optimized DTC control that takes advantage of the CDTC simplicity, and a reference torque compensation to force the torque to oscillate around the required value were proposed for three-phase and open-end winding PMSM. The proposed system mainly focuses on ripple reduction without adding too much complexity to the conventional DTC. To achieve the general objective of ripple reduction, duty ratio optimization that focuses on error square minimization was applied. In duty ratio optimization, the slope of the developed torque during active and null voltage periods is determined online. During duty ratio optimization, two sub-objectives were achieved. These objectives are torque error square minimization and making the developed torque of the motor equal to the reference torque at the end of the switching period. In conventional duty ratio optimization, the generated torque is usually below the reference torque and errors are one-sided. In order to reduce error magnitude, reference torque modification is performed in order to oscillate the developed torque on both sides of the reference. Compensation for the reference torque is based on the magnitude and sign of the torque error. In classical DTC, one voltage vector is used throughout the switching period, whereas the duty ratio is used to reduce ripple levels

TABLE 1. Comparison of different DTC strategies.

Strategy	Drawback and advantage
Conventional DTC (CDTC)	It has a simple algorithm, however, there are a lot of ripples, and the voltage is switched on throughout the switching period.
Space vector pulse width modulated DTC (DTC-SVM)	It has less ripple than CDTC, however, it is a more complex algorithm than CDTC.
Duty ratio optimized DTC based on torque error square minimization (DDTC-TESM)	It has less ripple and optimizes switching time. Although it is more sophisticated than CDTC, more computation is required to get the slope and duty ratio. The torque ranges from zero to a reference magnitude.
Maximum torque per ampere-based DTC (MTPA-DTC)	It optimizes the current magnitude for the required torque and improves efficiency. But it adds computation for the optimal current generation, torque ripple related to switching time is not considered.
Duty ratio optimized DTC based on current error square minimization (DDTC-CESM)	It has less ripple and implements optimal switching time. However, slope and duty ratio determination require more computation than CDTC. Torque range remains from minimum values to reference magnitude. Ripple remains on one side of the reference value. Duty ratio determination becomes complex even when both axis current is considered.
Model predictive based DTC (MP-DTC)	It improves response by enhancing one-step delay but adds computation complexity compared to CDTC. No optimal duty ratio is considered.
Duty ratio optimized DTC with voltage angle compensation (DDTC-VAC)	Reduce the torque ripple by optimizing the duty ratio and control the flux magnitude by adjusting the voltage phase angle. However, complicated angle and duty ratio calculations have been introduced.
Extended finite vector-based DTC (EFV-DTC)	Reduce the magnitude of ripple by varying the duty ratio from 0 to 1. It requires storing the torque and flux ripple for a set of finite duty ratios. The duty ratio is not optimal. Vector selection is based on data that is stored offline. This adds complexity.
Midpoint saturation DTC (MPS-DTC)	Reduce the magnitude of ripple by varying the duty ratio from 0 to 1. However, the duty ratio is not the optimal one, and the calculation of the duty ratio for zero error magnitude is too difficult.
Nonlinear fuzzy-based control of d-axis current control for torque ripple minimization	In the idea proposed in this work, the only controlled variable is d-axis current. It doesn't consider the effect of the q-axis current. The fuzzy decision is based on span length and the accuracy of the decision is low.
Optimal constant frequency switched pulse width modulated DTC (OTPWM-DTC)	This scheme reduces the torque error to zero at the end of the switching period, but the optimal switching time calculation is complex as two active voltages are used. The number of commutes is high.
Minimum voltage vector error-based DTC (MVVE-DTC)	A vector is selected based on the response required, but it is applied for the total switching time, and there is no concept of duty ratio optimization.
Optimized duty ratio-based DTC with torque compensation	This is the proposed one. The proposed control strategy involves simplicity similar to CDTC, duty ratio optimization to reduce the ripple magnitude, and compensation of the reference torque to control torque around the desired value from both sides. Here error compensation is added to divide the ripple on both sides of the reference torque. This reduces both the magnitude of the ripple and the sum of the error squares. A torque squared minimization method is used to determine the duty ratio. Two objectives were achieved with the proposed method for duty ratio. The first objective is the minimization of errors, and the second objective is ensuring that the torque is equal to the reference torque at the end of the switching span. In addition, the voltage vector is chosen to give a fast dynamic response.

by optimizing the switching time of the active voltage. The ripple oscillation is limited to one side of the reference torque in this scheme. While in this work, error compensation is used to divide the ripple into two sides of the reference torque. This

reduces the magnitude of the ripple and the error square sum. The mathematical importance of this scheme compared to the duty ratio without compensation is presented in the ripple reduction analysis section.

II. MATHEMATICAL MODEL OF PMSM AND METHOD

A. MATHEMATICAL MODEL OF PMSM

The equations depicted below were used to develop a simplistic two-axis model of a PMSM in the d-q axis frame.

$$V_q = Ri_q + \frac{d\psi_q}{dt} + \omega_s \psi_d \tag{1}$$

$$i_q = \frac{1}{L_q}\int (V_q - Ri_q - \omega_s \psi d)dt \tag{2}$$

$$V_d = Ri_d + \frac{d\psi_d}{dt} - \omega_s \psi_q \tag{3}$$

$$i_d = \frac{1}{L_d}\int (V_d - Ri_d - \omega_s \psi q)dt \tag{4}$$

$$\begin{cases} \psi_d = L_d i_d + m_f \\ \psi_q = L_q i_q \end{cases} \tag{5}$$

$$Te = 1.5P_n(\psi_d i_q - \psi_q i_d) \tag{6}$$

$$J\frac{d\omega_r}{dt} = T_e - T_L - B\omega_r \tag{7}$$

$$\omega_r = \frac{1}{J}\int (T_e - T_L - B\omega_r)dt \tag{8}$$

$$\omega_s = 0.5P_n\omega_r \tag{9}$$

$$\theta_r = \int \omega_s dt \tag{10}$$

Using Eq. (11), the d-q axis is transformed to the abc axis.

$$i_{abc} = \begin{bmatrix} \cos(\theta_r) & -\sin(\theta_r) \\ \cos(\theta_r - 2pi/3) & -\sin(\theta_r - 2pi/3) \\ \cos(\theta_r + 2pi/3) & -\sin(\theta_r + 2pi/3) \end{bmatrix} i_{dq} \tag{11}$$

The d-q is converted to the α-β axis using Eq. (12).

$$i_{\alpha\beta} = \begin{bmatrix} \cos(\theta_r) & -\sin(\theta_r) \\ \sin(\theta_r) & \cos(\theta_r) \end{bmatrix} i_{dq} \tag{12}$$

Transformation of abc to the d-q is done using Eq. (13), as shown at the bottom of the page.

B. DUTY RATION DETERMINATION METHOD

In this work, duty ratio optimized DTC control that takes advantage of CDTC simplicity and reference torque compensation was proposed for three-phase and open-end winding PMSM. To achieve the general objective of ripple reduction, duty ratio optimization that focuses on error square minimization was applied. The active and null voltage

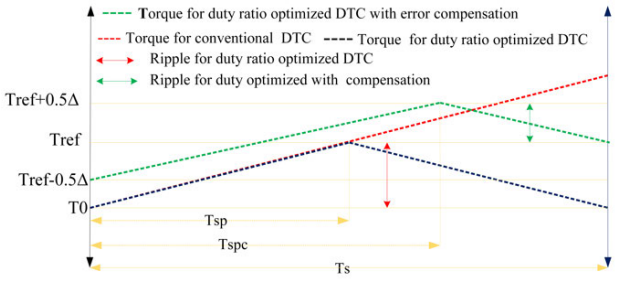

FIGURE 1. Illustrates the duty optimization method and torque compensation, when the red dotted line represents torque response without duty ratio optimization, the black dotted line represents torque response with duty ratio optimization, and the green dotted line represents torque for the compensated duty ratio optimized method.

periods' slopes were calculated using Eq. (16) and Eq. (17) respectively, where S1 and S0 are the active and null voltage periods' torque slopes, respectively.

$$\frac{d\psi_d}{dt} = V_d - \left(Ri_d - \omega_s \psi_q\right) \tag{14}$$

$$\frac{di_q}{dt} = \frac{1}{L_q}\left(V_q - Ri_q - \omega_s \psi_d\right) \tag{15}$$

$$S_1 = 1.5P_n\left(\frac{d\psi_d}{dt}i_q + \frac{di_q}{dt}\psi_d\right) \quad \text{for } 0 < t < T_{sp} \tag{16}$$

$$S_0 = 1.5P_n\left(\frac{d\psi_d}{dt}i_q + \frac{di_q}{dt}\psi_d\right) \quad \text{for } T_{sp} < t < T_s \tag{17}$$

Fig. 1 depicts the optimization and compensation of the error torque used in this study, where T_{ref} denotes the reference torque, Δ denotes the difference between the reference torque and the developed torque, T_0 denotes the magnitude of the torque at the start of the period, Ts denotes the total switching period, T_{sp} denotes the optimal switching time for the duty ratio optimized case, and T_{SPC} denotes the optimal switching time for the compensated system.

Torque change is calculated by comparing the reference torque to the actual torque at any particular time. The formula for developed torque shown by the black dotted line in Fig. 1 can be represented as shown in the equation below.

$$Te = \begin{cases} T_0 + S1t & \text{for } 0 < t < T_{sp} \\ T_{ref} + S0(t - T_{sp}) & \text{for } T_{sp} < t < T_s \end{cases} \tag{18}$$

The equation for switching time is found by minimizing the sum of the torque error squares.

$$\frac{d}{dT_{sp}}\left(\sum_0^{Ts}\Delta^2\right) = \frac{d}{dT_{sp}}\left(\int_0^{Ts}(Tref - Te)^2\,dt\right) = 0 \tag{19}$$

Solving the above equation, the expression for the switching period is obtained.

$$T_{sp} = \frac{T_{ref} - T_o + S0T_s}{S1 - S0} \tag{20}$$

$$idq = \frac{2}{3}\begin{bmatrix} \cos(\theta_r) & \cos(\theta_r - 2pi/3) & \cos(\theta_r + 2pi/3) \\ -\sin(\theta_r) & -\sin\cos(\theta_r - 2pi/3) & -\sin\cos(\theta_r + 2pi/3) \end{bmatrix} iabc \tag{13}$$

An active voltage is utilized for periods less than Tsp, whereas the null voltage is used to minimize ripple for periods between Tsp and Ts. The torque reference can be adjusted so that the developed torque oscillates about the required torque from both sides. The required torque is greater than the motor's torque if the torque error is positive. This means that to raise the electromagnetic torque, the duty ratio must be increased. When the reference torque is used as it is, the optimal duty will be reached when the developed torque is equal to the reference torque. However, once the instant torque exceeds the reference torque, it drops, and most of the time, the torque falls below the reference torque. To improve this, the reference torque is adjusted for both negative and positive torques. The equation for the magnitude of the reference torque after compensation is obtained by the following equation, when Trefc is the magnitude of the reference after compensation, and sign is the sign of an error.

$$T_{refc} = T_{ref} + 0.5sign(\Delta) \times |\Delta| \tag{21}$$

C. ANALYSIS OF RIPPLE REDUCTION

This section presents the mathematical justification of the proposed scheme compared to the conventional duty ratio optimization method. For comparison of the effectiveness of the method, the magnitude of the ripple square sum is used. For the dotted green color graph in Fig.1, the equation for the line can be expressed by Eq. (22). The magnitude of the sum of the error squares can be obtained using the expression shown in Eq. (23).

$$T = \begin{cases} Tref - \dfrac{\Delta}{2} + S1t, & \text{for } 0 < t < Tspc \\ Tref + \dfrac{\Delta}{2} + S0t, & \text{for } Tspc < t < Ts \end{cases} \tag{22}$$

The sum of the error square between the reference torque and the developed torque is obtained by using the equation below.

$$\sum_{0}^{Ts} error^2 = \begin{pmatrix} \int_0^{Tspc} \left(Tref - (Tref - \dfrac{\Delta}{2} + S1t) \right)^2 dt \\ + \int_{Tspc}^{Ts} (Tref - (Tref + \dfrac{\Delta}{2} + S0t))^2 dt \end{pmatrix} \tag{23}$$

Simplifying the Eq. (23), the following equation was obtained.

$$\sum_{0}^{Ts} error^2 = \begin{pmatrix} \int_0^{Tspc} \left(\dfrac{\Delta^2}{4} - S1\Delta \times t + S1^2t^2 \right) dt \\ + \int_{Tspc}^{Ts} (\dfrac{\Delta^2}{4} + S0\Delta \times t + S0^2t^2) dt \end{pmatrix} \tag{24}$$

Integration of the Eq. (24) results in the expression shown in Eq. (25).

$$\sum_{0}^{Ts} error^2 = \begin{matrix} \left[\dfrac{\Delta^2 t}{4} - \frac{S1\Delta t^2}{2} + \dfrac{S1^2t^3}{3} \right]_{t=0}^{Tspc} + \\ \left[\dfrac{\Delta^2 t}{4} + \frac{S0\Delta t^2}{2} + \dfrac{S0^2t^3}{3} \right]_{t=Tspc}^{Ts} \end{matrix} \tag{25}$$

Collecting like terms and cancelling the terms which consist of t^2 and t^3 the following simple equation was obtained for the sum of error squares for the compensated case. The values of switching time square, optimal switching time square, and the cube of these values are very small. Thus, the dominant terms can be expressed as shown below assuming the constant term to be zero during integration.

$$\sum_{0}^{Ts} error^2 = \left[\frac{\Delta^2 t}{4} \right]_{t=0}^{Tspc} + \left[\frac{\Delta^2 t}{4} \right]_{t=Tspc}^{Ts} \tag{26}$$

Further manipulating and substituting the values of the variables in Eq. (26), the result for the sum of torque error square is obtained as it is shown in Eq. (27).

$$\sum_{0}^{Ts} error^2 \approx \frac{Ts\Delta^2}{4} \tag{27}$$

where the variable Δ is the difference between the reference torque and the lower limit of the developed torque. For a switching period of 0.001 seconds and a ripple range of 0.1Nm, the value of Eq. (27) is 0.0000025.

For the uncompensated duty ratio optimized case, the equation for the blue dotted line depicted in Fig. 1, which represents motor torque within the allowable range can be expressed as shown below.

$$T = \begin{cases} T0 + S1t, & \text{for } 0 < t < Tsp \\ Tref + S0t, & \text{for, } Tsp < t < Ts \end{cases} \tag{28}$$

The sum of the error square between the reference torque and the developed torque is obtained by using the equation below.

$$\sum_{0}^{Ts} error^2 = \begin{pmatrix} \int_0^{Tspc} (Tref - (T0 + S1t))^2 dt \\ + \int_{Tspc}^{Ts} (Tref - (Tref + +S0t))^2 dt \end{pmatrix} \tag{29}$$

Simplifying Eq. (29) and expanding the terms in brackets, the following equation was obtained.

$$\sum_{0}^{Ts} error^2 = \begin{pmatrix} \int_0^{Tspc} (Tref^2 - 2Tref(T0 + S1t) + T0^2 \\ + (2S1T0)t + S1^2t^2) dt + \int_{Tspc}^{Ts} S0^2t^2 dt \end{pmatrix} \tag{30}$$

An integration of the Eq. (30) gives the following expression for the sum of the error square.

$$\sum_{0}^{Ts} error^2 = \begin{cases} \left[Tref^2 t - 2(Tref \times T0)t \right]_{t=0}^{Tspc} \\ + \left[S1t^2(T0 - Tref) + T0^2 t \right]_{t=0}^{Tspc} \\ + \left[\dfrac{S1^2t^3}{3} \right]_0^{Tspc} + \left[\dfrac{S0^2t^3}{3} \right]_{t=Tspc}^{Ts} \end{cases} \tag{31}$$

Eliminating the term which consists of the expressions t^2 and t^3 as the variable t indicates the time between 0 to the switching period, the square and cube of the variable become

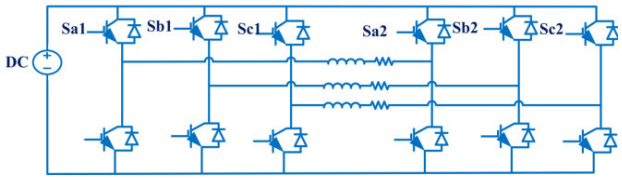

FIGURE 2. OEW PMSM supplied from single inverter.

a very small number. So, the expression in Eq. (31) can be written as shown below by eliminating terms with t^2 and t^3.

$$\sum_{0}^{Ts} error^2 = \left[Tref^2 t - 2(T0 \times Tref)t + T0^2 t\right]_{t=0}^{Tspc} \quad (32)$$

The expression in Eq. (32) can be rewritten as shown in Eq. (33).

$$\sum_{0}^{Ts} error^2 = \left[(Tref - T0)^2 t\right]_{t=0}^{Tspc} \quad (33)$$

As the variables Δ is defined the difference between Tref and T0, the expression in Eq. (33), can be substituted by this variable.

$$\sum_{0}^{Ts} error^2 = \left[\Delta^2 t\right]_{t=0}^{Tspc} \quad (34)$$

Substituting and evaluating the expression in Eq. (34), the approximate value of the sum of torque errors squared is obtained by Eq. (35). So dominant terms can be expressed as shown below assuming the constant term to be zero during integration.

$$\sum_{0}^{Ts} error^2 \approx \Delta^2 Tsp \quad (35)$$

The value of the variable Tsp ranges from zero to Ts. When a value of Tsp is greater than 0.25 Ts, the magnitude of the sum square error for the compensated system is less than the uncompensated one. For a switching period of 0.001 seconds and a ripple range of 0.1, taking the value of Tsp as Ts, the value of Eq. (35) is 0.00001. This means compensation reduces the error square sum by four times.

III. OVERVIEW OF THREE-PHASE OEW PMSM

OEW three-phase PMSM was used to obtain high power when two independent sources were used. By altering the ratio of both terminal DC voltages, the OEW method can provide multilevel voltage [21], [22]. The diagram in Fig. 2 shows the schematic for OEW PMSM.

The magnitude of the phase voltage can be evaluated using the following Eq. (36) when Vdc is the supply DC voltage and the variables in Fig. 2 denotes the switching signal for the top switches for each inverter. The switching signal has a value of one or zero.

$$Vabc_{OEW} = {}^{Vdc}/_{3} \begin{bmatrix} 2 & -1 & -1 \\ -1 & 2 & -1 \\ -1 & -1 & 2 \end{bmatrix} \begin{bmatrix} Sa1 - Sa2 \\ Sb1 - Sb2 \\ Sc1 - Sc2 \end{bmatrix} \quad (36)$$

TABLE 2. Lookup table for DTC.

Voltage vector selection strategy							
For three-phase PMSM							
φ	T	S1	S2	S3	S4	S5	S6
1	1	V2	V3	V4	V5	V6	V1
	0	V7	V8	V7	V8	V7	V8
	-1	V6	V1	V2	V3	V4	V5
0	1	V3	V4	V5	V6	V1	V2
	0	V8	V7	V8	V7	V8	V7
	-1	V5	V6	V1	V2	V3	V4
For OEW PMSM							
φ	T	S1	S2	S3	S4	S5	S6
1	1	V35*	V46*	V51*	V62*	V13*	V24*
	-1	V13*	V24*	V35*	V46*	V51*	V62*
0	1	V46*	V51*	V62*	V13*	V24*	V35*
	-1	V62*	V13*	V24*	V35*	V46*	V51*

TABLE 3. Motor parameter.

Parameter	Magnitude	Parameter	Magnitude
Ls	10.5mH	R	1.12ohm
fs	1khz	Pole	4
flux	0.725wb	Rated speed	1500 rpm

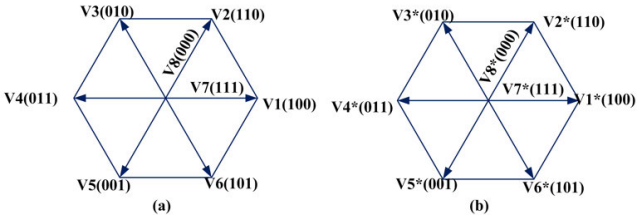

FIGURE 3. (a) Shows the switching state of the first inverter, (b) shows the switching state of the second inverter.

The Y-connected scheme is obtained by isolating the second inverter and shorting the three phases together. The magnitude of voltage in this case is obtained by Eq. (37).

$$Vabc = {}^{Vdc}/_{3} \begin{bmatrix} 2 & -1 & -1 \\ -1 & 2 & -1 \\ -1 & -1 & 2 \end{bmatrix} \begin{bmatrix} Sa1 \\ Sb2 \\ Sc3 \end{bmatrix} \quad (37)$$

For torque and flux, a three-level hysteresis regulator and a two-level hysteresis regulator are used in traditional DTC. The simple lookup table introduced in [22] is employed for the OEW method.

Table 2, the notation ab* indicates the switching states of the inverters. When a represents the state of the first inverter and b* represents the state of the second inverter. This work uses a conventional lookup table. However, the novelty lies in the application of duty ratio and torque error compensation.

The constant torque and constant speed operations are addressed during the simulation. For constant speed operation, the speed was set to 477.5 rpm and the torque was changed from 4 Nm to 8 Nm at 0.25. For constant torque,

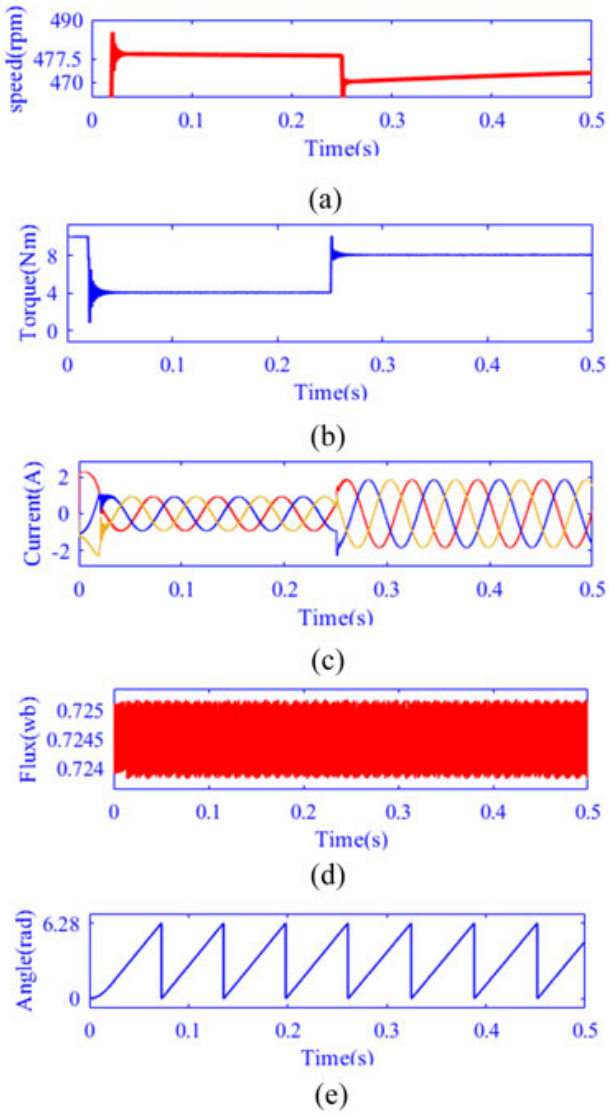

FIGURE 4. Shows a three-phase PMSM response with a proposed control system at a constant speed and variable torque when (a) shows the speed, (b) shows the torque, (c) shows the current waveform, (d) shows the magnitude of flux, and (e) shows the flux angle.

the torque was set to 4 Nm and the speed was changed from 477.5 rpm to 238.75 rpm at 0.25 seconds. The motor rating used in this work is depicted in Table 3.

IV. SIMULATION RESULT AND DISCUSSION

The Matlab 2021b Simulink environment is used for simulation purposes. During the simulation, variable torque and variable speed were addressed. The simulation covers constant speed operation conditions, constant torque operation, and four-quadrant operation. In constant speed operation, the load torque is varied and the responses are observed. While under constant load, the speed is varied and the effectiveness of the scheme is observed. In four quadrants of operation of the drive, the scheme is checked for its effectiveness during both motoring and braking.

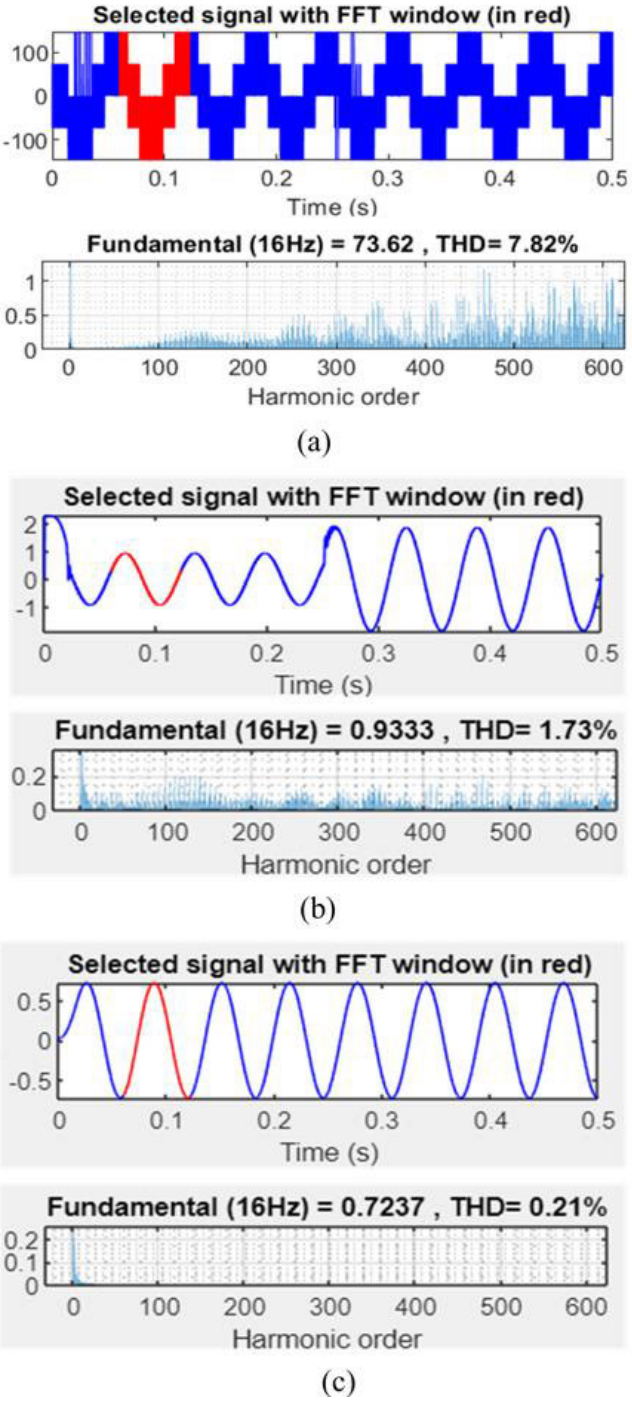

FIGURE 5. Shows harmonic at 477.5 rpm and 4 Nm when (a) shows the voltage harmonic, (b) shows the current harmonic, (c) shows the flux harmonic.

A. CONSTANT SPEED OPERATION OF PMSM

In this scheme, the reference speed was kept constant and the load torque was changed in step fashion.

Fig.4 shows that the proposed scheme performs well in terms of speed dynamics, torque dynamics, current waveforms, and flux variations. Both the rising and settling

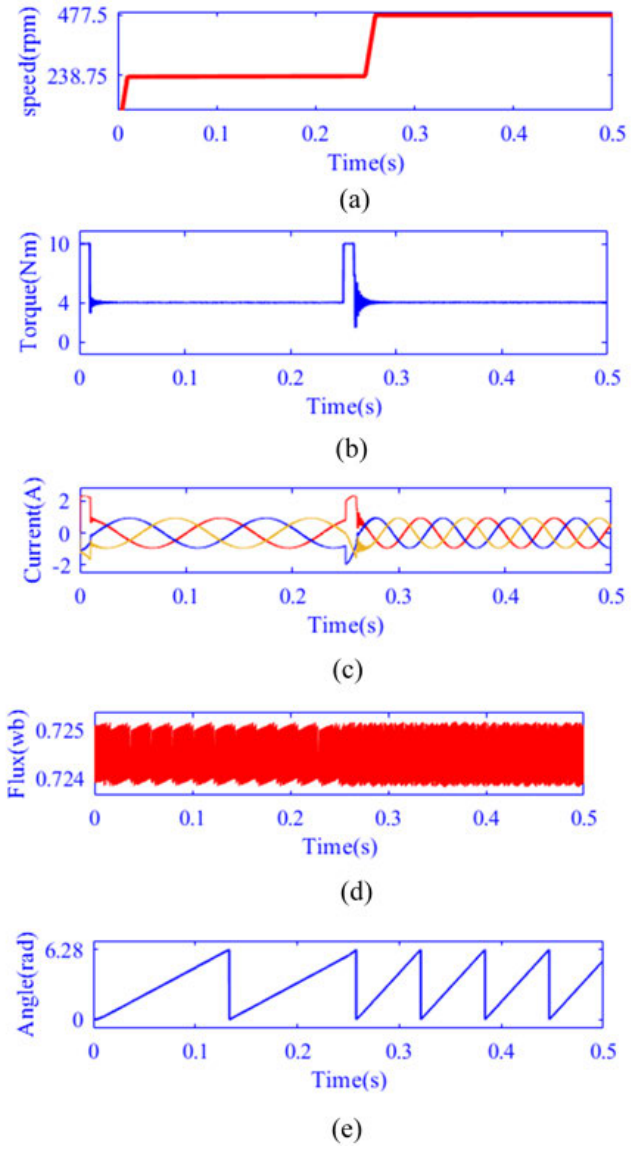

FIGURE 6. Shows a three-phase PMSM response with a proposed control system at a constant torque and variable speed (a) shows the speed, (b) shows the torque, (c) shows the current waveform, (d) shows the magnitude of flux, (e) shows the flux angle.

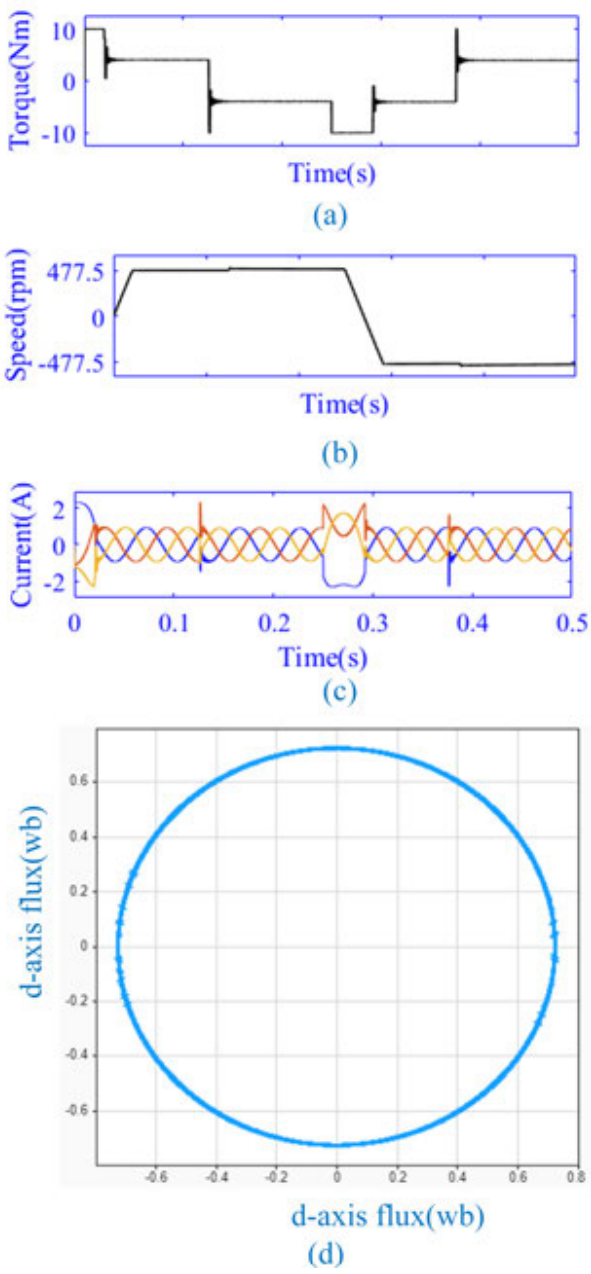

FIGURE 7. Shows the response in four quadrant operation when, (a) shows the torque response, (b) shows the speed response, (c) shows the stator current waveform, (d) shows the flux plot.

times are very short for speed and torque. The current waveform is also good. In addition, the flux variation is also minimal. Fig.5 shows voltage, current, and flux harmonics with a selected FFT window.

The diagram in Fig.5, shows the harmonic with FFT window for voltage, current, and flux. The voltage THD, current THD, and flux THD are 7.82%, 1.73%, and 0.21% respectively. This indicates superior performance in terms of harmonic performance.

B. CONSTANT TORQUE OPERATION OF PMSM

In simulations, the result of compensated optimized duty ratio DTC control of PMSM is depicted in Fig. 4, Fig. 5, and Fig. 6. The simulation result in Fig. 4 (a) shows that the speed response for constant speed and variable torque has an overshoot of 1.6%, and almost zero steady-state error. Additionally, the torque response shown in Fig. 4(b) has almost zero steady-state error. While in Fig. 4(c) the flux error varies with only a small deviation and the flux ripple is less in high-speed range. The harmonic content depicted in Fig. 5 demonstrates that the scheme is effective in terms of harmonic performance. In the diagram depicted in Fig. 6, the performance of the control scheme for variable speed was presented. It was seen that the speed, torque and flux performance are good.

C. FOUR QUADRANTS OPERATION OF PMSM

The speed and torque sign depend upon the mode of operation or the quadrant in which the motor is operating. In Fig.7, from the time 0 to 0.125 seconds, both torque and speed are positive. While from 0.125 to 0.25 seconds torque is negative and speed is positive. While from the time 0.25 to 0.375 seconds, both torque and speed are negative. And finally, from the time 0.375 to 0.5 seconds, torque is positive and speed is negative. This simulation covers all four quadrants.

Fig.7 shows that drive response is effective in all quadrants.

D. CONSTANT SPEED OPERATION OF OEW PMSM

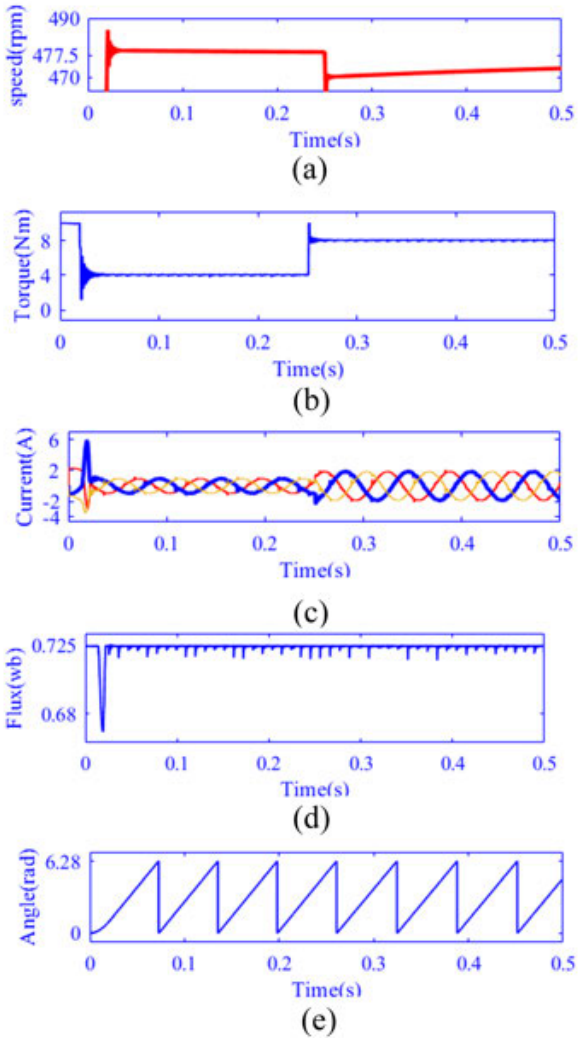

FIGURE 8. Shows a three-phase OEW PMSM response with a proposed control system at a constant speed and variable torque (a) shows the speed, (b) shows the torque, (c) shows the current, (d) shows the magnitude of flux, (e) shows the flux angle.

E. CONSTANT TORQUE OPERATION OF OEW PMSM

The simulation result of compensated optimized duty ratio DTC control of OEW PMSM is depicted in Fig. 8, Fig. 9,

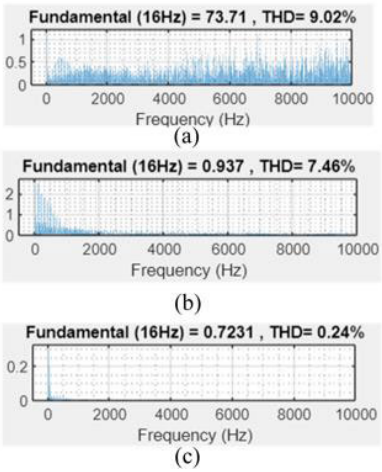

FIGURE 9. Shows harmonic at 477.5 rpm and 4 Nm when (a) shows the voltage harmonic, (b) shows the current harmonic, (c) shows the flux harmonic for three-phase OEW PMSM.

and Fig. 10. The simulation result in Fig. 8 (a) shows that the speed response for constant speed and variable torque has an overshoot of 1.6%, and almost zero steady-state error. Additionally, the torque response shown in Fig. 8(b) has almost zero steady-state error. Whereas in Fig. 10(d) the flux error varies with speed and the flux ripple is less in high-speed ranges. The flux variation is high at low speed and light load in the case of OEW PMSM. The harmonic content depicted in Fig. 9 indicates that this scheme is effective in terms of harmonic performance. In the diagram depicted in Fig. 10, the performance of the control scheme for variable speed was presented. The torque, speed, and flux performance are acceptable, but the flux variation and current wave distortion are high at low speeds and light loads. The results in Fig. 10(c) and Fig.10 (d) indicate that at lower speeds and light loads, the performance of OEW PMSM is less than normal three phase PMSM. The current harmonic contributes a lot to the heating of the motor winding. This heating effect can be measured as the ratio of power loss due to harmonics to total power loss. This ratio can be calculated using Eq. (39) shown below.

$$I_{THD} = \frac{\sum_{n=2}^{\infty} I_n^2}{I_1} \tag{38}$$

Using the relation in Eq. (38), the ratio of power loss due to harmonic to total power is calculated using equation Eq. (39) depicted below.

$$\frac{P_{lossh}}{p_{lossT}} = \frac{I_{THD}^2}{(1 + I_{THD})^2} \tag{39}$$

F. FOUR QUADRANTS OPERATION OF OEW PMSM

Motor speed and torque are determined by the mode of operation or by the quadrant in which it operates.

In Fig.11, the simulation covers all four quadrants for OEW PMSM. It can be seen in this figure that the scheme is

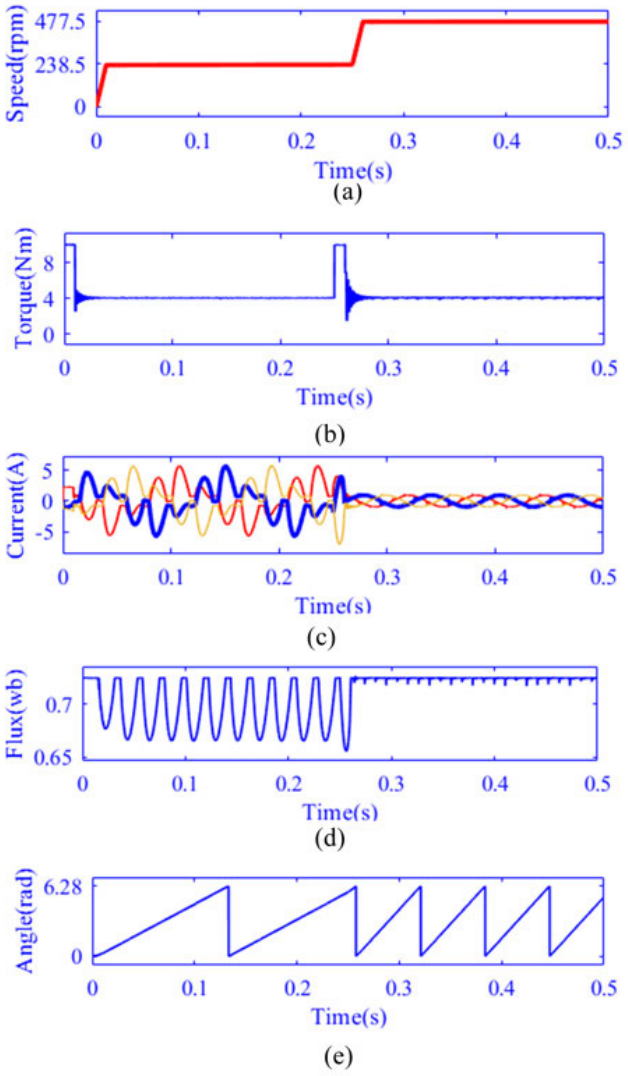

FIGURE 10. Shows a three-phase OEW PMSM response with a proposed control system at a constant torque and variable speed (a) shows the speed, (b) shows the torque, (c) shows the current waveform, (d) shows the magnitude of flux, (e) shows the flux angle.

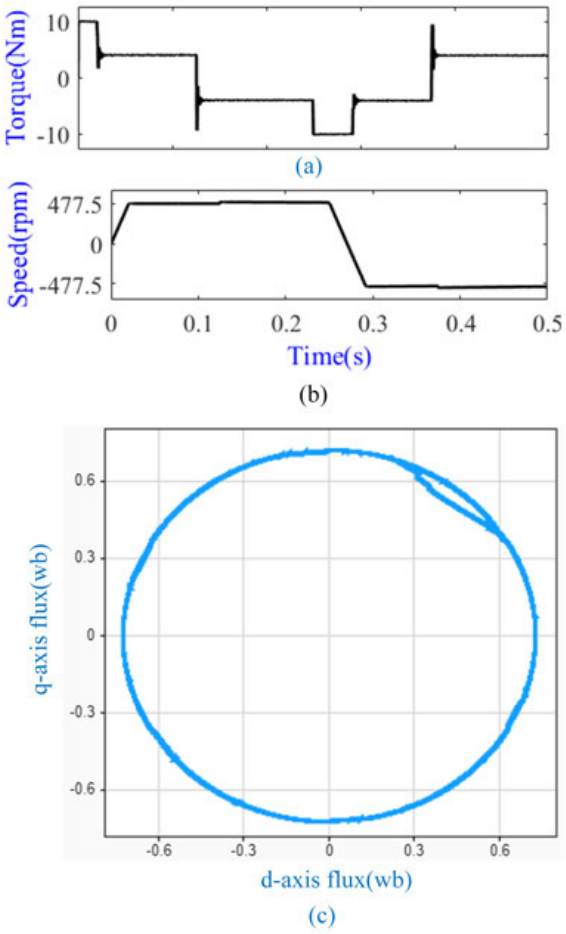

FIGURE 11. Shows the response in four quadrant operation when, (a) shows the torque response, (b) shows the speed response, (c) shows the flux plot.

effective in all quadrants for OEW PMSM. Both cases exhibit high-accuracy torque responses. As it is shown in Fig. 5(b) and Fig. 9(b), the current harmonics at 477.5 rpm and 4 Nm are 1.73 % and 7.46% respectively for the normal three-phase and OEW PMSM scheme. Using Eq. (39), the value of the ratio of power loss due to harmonics to total power is 0.025% and 4.8% for three-phase PMSM in normal and OEW schemes respectively. The proposed system has the best current performance for three-phase PMSM. Fig. 5 and Fig. 9 depicts the voltage harmonic, current harmonic, and flux harmonic at 477.5 rpm and a load torque of 4 Nm. In Fig. 5, the voltage harmonic, current harmonic and flux harmonic are 7.82%, 1.73%, and 0.21% respectively. Whereas in the case of OEW PMSM, the simulation result in Fig.9 indicates the voltage harmonic, current harmonic, and flux are 9.02%, 7.46%, and 0.24% respectively.

Compared to the work presented for the duty ratio optimized scheme in [17], the performance of the proposed scheme is effective. In the work presented in [17], the current harmonic is 10%. For the proposed scheme in this work, the current harmonic illustrated in Fig. 5(b) and Fig. 9(b) are 1.73% and 7.46% respectively for PMSM and OEW PMSM respectively. This indicates that the scheme is effective for both PMSM and OEW PMSM. In addition, in the work reported in [21], the current harmonic is 9.8%. This means the proposed scheme has better harmonic performance than the work reported in [21]. The work in [22] also presented the duty ratio performance of PMSM. This work has a harmonic of 9.77%. Compared to the work presented in [22], the harmonic performance of the proposed scheme is better.

In the work presented in [23], where two separate vectors were used for ripple reduction of flux and torque ripple, the harmonic performance was 18.01%. So compared to this work, the proposed scheme has better performance. Again, in the work presented in [24], where the two independent cost functions are used for duty ratio determination, the

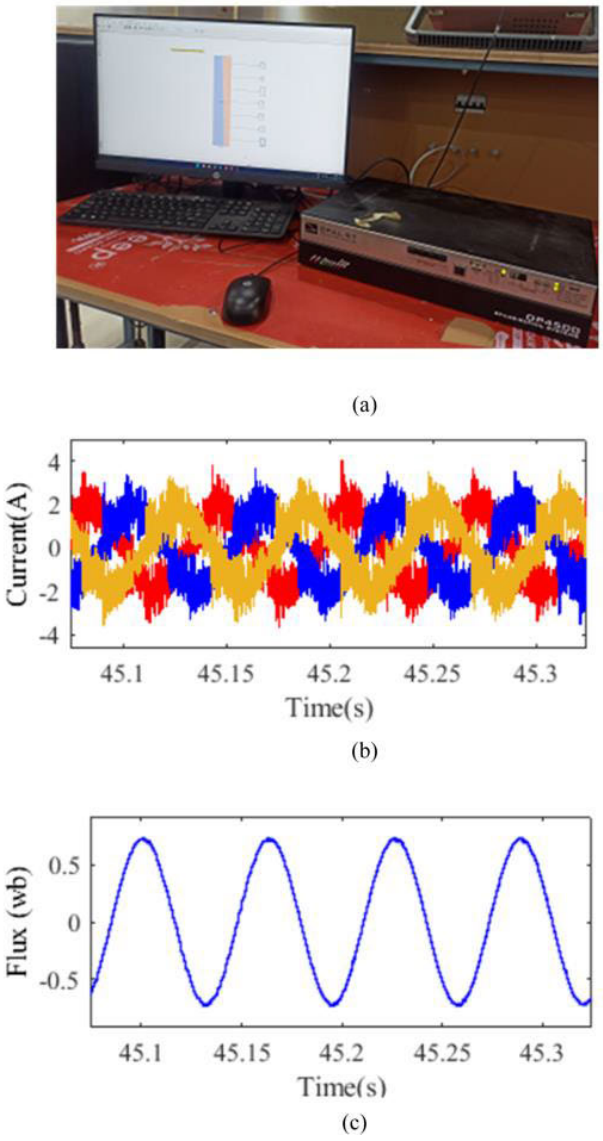

FIGURE 12. (a) Shows the real-time simulator setup, (b) indicates the current waveform, and (c) indicates the flux waveform.

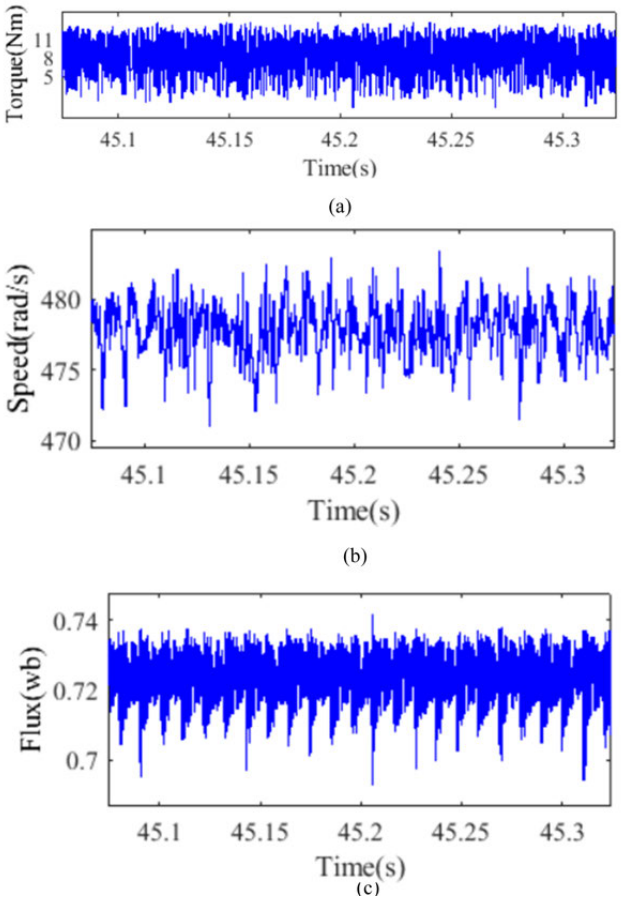

FIGURE 13. (a) Indicates torque, (b) indicates speed response, and (c) indicates flux magnitude.

harmonic performance at 20 rpm and 16 Nm is 10.68%. So compared to this work also the harmonic performance is of the proposed scheme is better. The shortcoming of this method for the OEW scheme is the generation of the 5th and 7th harmonics. The proposed method is effective for three-phase normal PMSM compared to the OEW scheme in reducing the ratio of power loss due to harmonics to total power. Further, the diagrams in Fig.7 and Fig.11 indicate that the scheme is equally effective for motoring as well as braking. These figures indicate that the scheme works fine in all quadrants based on speed dynamics, torque dynamics, and flux plots.

V. EXPERIMENTAL VERIFICATION

There is a power circuit and a control circuit in the total drive system. Integrated gate driven IGBTs and sensors provide isolation between the power and control circuits. The controller used for control purposes is determined by the level of switching frequency required. Based on the number of pulses measured, the resolution of the encoder for one revolution, and the switching time, the magnitude of the sensed speed is determined. Providing appropriate mechanical protection and selecting the right sensor rating can ensure proper protection. Control scheme effectiveness is tested with Hardware in Loop (HIL). The general layout of the HIL system used in this work is depicted in Fig.12. OPAL-RT works in two modes. These modes are software and hardware synchronized. In this work, the software-synchronized mode is used to test the effectiveness of the control scheme. RT-Lab 2021.3 and Matlab 2018a were used to compile and run the model on OP4500.

The diagram in Fig. 12 (b) and Fig. 12 (c) shows the waveform of three phase current and flux taken at load of 8Nm, and speed of 477.5 rpms respectively.

The quantitative performance of the proposed scheme obtained from a real time simulator indicates that the scheme is effective. Fig.13 show the torque, speed and flux taken at load of 8Nm and speed of 477.5 rpms. The results indicate that the scheme is effective. The ripple magnitude is 0.5%,

0.014%, and 37.5% percent for speed, flux, and torque respectively.

VI. COMPARISON OF EXPERIMENTAL AND SIMULATION RESULTS

Fig. 4(c), Fig. 6(c), Fig. 7 (c) and Fig. 8 (c) shows the current waveform result obtained from the simulation for the PMSM controlled by the proposed scheme. Compared to the experimental results presented in Fig. 12 (b), the simulation result has less ripple. Additional key factors for comparison are torque ripple, speed ripple and flux ripple. Fig. 4(b), Fig. 6(b), Fig. 7 (a), Fig. 8 (b), Fig. 10 (b) and Fig. 11 (a) shows the torque result obtained from the simulation for the PMSM controlled by the proposed scheme. Compared to the experimental results presented in Fig. 13 (a), the simulation result has less ripple.

Fig. 4(a), Fig. 6(a), Fig.7 (b), Fig. 8(a), Fig. 9(a), Fig. 10(a) and Fig. 11 (b) shows the speed result obtained from the simulation for the PMSM controlled by the proposed scheme. Compared to the experimental results presented in Fig. 13 (b), the simulation result has less ripple. Fig. 4(d), Fig. 6(d) and Fig. 8 (d) shows the flux result obtained from the simulation for the PMSM controlled by the proposed scheme. Compared to the experimental results presented in Fig. 13 (c), the simulation result has less ripple. The results in both cases indicate that the scheme works well.

VII. CONCLUSION

In this work, the compensated duty ratio optimized DTC control, which has the simplicity of CDTC and torque compensation of reference torque to enforce the torque to oscillate around the required value, was proposed. The slope was obtained by considering the torque error minimization and pushing the produced torque to be equal to the reference torque at the span's end. In normal conditions, the proposed control technique was applied to three-phase PMSM and open-end wind schemes. The proposed scheme is very effective for three-phase PMSM in terms of ripple and harmonic performance. In the case of an open-end winding scheme, the ripple performance is very good for torque and speed. However, the flux ripple is very high for open-end winding cases at low speed and light load. In addition, the total harmonic distortion is high due to the high magnitude of the fifth and seven harmonics in the case of open-end winding.

REFERENCES

[1] T. Guo, L. Deng, and Z. Miao, "Predictive direct torque control for permanent-magnet synchronous machines based on duty ratio modulation," *J. Phys., Conf.*, vol. 1311, no. 1, Sep. 2019, Art. no. 012041, doi: 10.1088/1742-6596/1311/1/012041.

[2] A. Shinohara, Y. Inoue, S. Morimoto, and M. Sanada, "Maximum torque per ampere control in stator flux linkage synchronous frame for DTC-based PMSM drives without using Q-axis inductance," *IEEE Trans. Ind. Appl.*, vol. 53, no. 4, pp. 3663–3671, Jul/Aug. 2017, doi: 10.1109/TIA.2017.2686800.

[3] G.-H. Zhou, M.-Z. Qiao, X.-F. Zhang, J.-H. Xie, Q.-L. Hao, C. Wan, and Y. Zhou, "Development of a low-speed high-efficiency PMSM and its drive system for electric windlass and mooring winch," *IEEE Access*, vol. 10, pp. 70620–70629, 2022, doi: 10.1109/ACCESS.2022.3149918.

[4] C. Sain, P. K. Biswas, P. R. Satpathy, T. S. Babu, and H. H. Alhelou, "Self-controlled PMSM drive employed in light electric vehicle-dynamic strategy and performance optimization," *IEEE Access*, vol. 9, pp. 57967–57975, 2021, doi: 10.1109/ACCESS.2021.3072910.

[5] Q. Liu and K. Hameyer, "Torque ripple minimization for direct torque control of PMSM with modified FCSMPC," *IEEE Trans. Ind. Appl.*, vol. 52, no. 6, pp. 4855–4864, Nov./Dec. 2016, doi: 10.1109/TIA.2016.2599902.

[6] C. Xia, S. Wang, X. Gu, Y. Yan, and T. Shi, "Direct torque control for VSI-PMSM using vector evaluation factor table," *IEEE Trans. Ind. Electron.*, vol. 63, no. 7, pp. 4571–4583, Jul. 2016, doi: 10.1109/TIE.2016.2535958.

[7] Z. Zhang, C. Wei, W. Qiao, and L. Qu, "Adaptive saturation controller-based direct torque control for permanent-magnet synchronous machines," *IEEE Trans. Power Electron.*, vol. 31, no. 10, pp. 7112–7122, Oct. 2016, doi: 10.1109/TPEL.2015.2511073.

[8] M. A. M. Cheema, J. E. Fletcher, D. Xiao, and M. F. Rahman, "A direct thrust control scheme for linear permanent magnet synchronous motor based on online duty ratio control," *IEEE Trans. Power Electron.*, vol. 31, no. 6, pp. 4416–4428, Jun. 2016, doi: 10.1109/TPEL.2015.2475400.

[9] M. H. Vafaie, B. M. Dehkordi, P. Moallem, and A. Kiyoumarsi, "A new predictive direct torque control method for improving both steady-state and transient-state operations of the PMSM," *IEEE Trans. Power Electron.*, vol. 31, no. 5, pp. 3738–3753, May 2016, doi: 10.1109/TPEL.2015.2462116.

[10] F. Niu, B. Wang, A. S. Babel, K. Li, and E. G. Strangas, "Comparative evaluation of direct torque control strategies for permanent magnet synchronous machines," *IEEE Trans. Power Electron.*, vol. 31, no. 2, pp. 1408–1424, Feb. 2016, doi: 10.1109/TPEL.2015.2421321.

[11] M. H. Vafaie, B. M. Dehkordi, P. Moallem, and A. Kiyoumarsi, "Improving the steady-state and transient-state performances of PMSM through an advanced deadbeat direct torque and flux control system," *IEEE Trans. Power Electron.*, vol. 32, no. 4, pp. 2964–2975, Apr. 2017, doi: 10.1109/TPEL.2016.2577591.

[12] Z. Zhang and X. Liu, "A duty ratio control strategy to reduce both torque and flux ripples of DTC for permanent magnet synchronous machines," *IEEE Access*, vol. 7, pp. 11820–11828, 2019, doi: 10.1109/ACCESS.2019.2892121.

[13] F. Niu, X. Huang, L. Ge, J. Zhang, L. Wu, Y. Wang, K. Li, and Y. Fang, "A simple and practical duty cycle modulated direct torque control for permanent magnet synchronous motors," *IEEE Trans. Power Electron.*, vol. 34, no. 2, pp. 1572–1579, Feb. 2019, doi: 10.1109/TPEL.2018.2833488.

[14] X. Lin, W. Huang, W. Jiang, Y. Zhao, and S. Zhu, "Deadbeat direct torque and flux control for permanent magnet synchronous motor based on stator flux oriented," *IEEE Trans. Power Electron.*, vol. 35, no. 5, pp. 5078–5092, May 2020, doi: 10.1109/TPEL.2019.2946738.

[15] S. J. Kim, J.-W. Kim, B.-G. Park, and D.-H. Lee, "A novel predictive direct torque control using an optimized PWM approach," *IEEE Trans. Ind. Appl.*, vol. 57, no. 3, pp. 2537–2546, May 2021, doi: 10.1109/TIA.2021.3060693.

[16] J. Hang, S. Ding, X. Ren, Q. Hu, Y. Huang, W. Hua, and Q. Wang, "Integration of interturn fault diagnosis and torque ripple minimization control for direct-torque-controlled SPMSM drive system," *IEEE Trans. Power Electron.*, vol. 36, no. 10, pp. 11124–11134, Oct. 2021, doi: 10.1109/TPEL.2021.3073774.

[17] A. Nasr, C. Gu, X. Wang, G. Buticchi, S. Bozhko, and C. Gerada, "Torque-performance improvement for direct torque-controlled PMSM drives based on duty-ratio regulation," *IEEE Trans. Power Electron.*, vol. 37, no. 1, pp. 749–760, Jan. 2022, doi: 10.1109/TPEL.2021.3093344.

[18] X. Wu, W. Huang, X. Lin, W. Jiang, Y. Zhao, and S. Zhu, "Direct torque control for induction motors based on minimum voltage vector error," *IEEE Trans. Ind. Electron.*, vol. 68, no. 5, pp. 3794–3804, May 2021, doi: 10.1109/TIE.2020.2987283.

[19] B. A. Basit, H. H. Choi, and J.-W. Jung, "An online torque ripple minimization technique for IPMSM drives: Fuzzy system-based D-axis current design approach," *IEEE Trans. Ind. Electron.*, vol. 68, no. 12, pp. 11794–11805, Dec. 2021, doi: 10.1109/TIE.2020.3044807.

[20] A. G. de Castro, P. R. U. Guazzelli, C. M. R. de Oliveira, W. C. D. A. Pereira, G. T. de Paula, and J. R. B. D. A. Monteiro, "Optimized current waveform for torque ripple mitigation and MTPA operation of PMSM with back EMF harmonics based on genetic algorithm and artificial neural network," *IEEE Latin Amer. Trans.*, vol. 18, no. 9, pp. 1646–1655, Sep. 2020, doi: 10.1109/TLA.2020.9381808.

[21] M. Wang, D. Sun, W. Ke, and H. Nian, "A universal lookup table-based direct torque control for OW-PMSM drives," *IEEE Trans. Power Electron.*, vol. 36, no. 6, pp. 6188–6191, Jun. 2021, doi: 10.1109/TPEL.2020.3037202.

[22] X. Lin, W. Huang, W. Jiang, Y. Zhao, D. Dong, and X. Wu, "Direct torque control for three-phase open-end winding PMSM with common DC bus based on duty ratio modulation," *IEEE Trans. Power Electron.*, vol. 35, no. 4, pp. 4216–4232, Apr. 2020, doi: 10.1109/TPEL.2019.2935295.

[23] S. G. Petkar and V. K. Thippiripati, "A novel duty-controlled DTC of a surface PMSM drive with reduced torque and flux ripples," *IEEE Trans. Ind. Electron.*, vol. 70, no. 4, pp. 3373–3383, Apr. 2023, doi: 10.1109/TIE.2022.3181405.

[24] R. E. K. Meesala, A. Srivastava, S. Bindu, and S. Chakraborty, "An enhanced electric vehicle with modified predictive direct torque control of open winding permanent magnet synchronous motor drive," in *Proc. IEEE Global Conf. Comput., Power Commun. Technol. (GlobConPT)*, Sep. 2022, pp. 1–6, doi: 10.1109/GlobConPT57482.2022.9938311.

BERHANU DEGGEFA LEMMA was born in Diksis, Ethiopia, in 1988. He received the B.Sc. and M.Sc. degrees from Adama Science and Technology University, in 2012 and 2017, respectively. From 2012 to 2019, he taught with Dire Dawa University, Ethiopia. Currently, he is a Research Scholar with the National Institute of Technology Warangal (NITW). He is also working on a PMSM drive. He has published journals and presented a paper at the international conferences.

SRINIVASAN PRADABANE (Member, IEEE) was born in Puducherry, India, in 1983. He received the Graduate degree from Pondicherry University, in 2005, the master's degree from Anna University, in 2008, and the Ph.D. degree from the National Institute of Technology Warangal, in 2016. He did his postdoctoral research in the U.K., in 2021. He has published many articles in reputable journals. His research interests include multilevel inverters, PWM schemes, induction motor drives, electric vehicles, integration of renewable, DC motor drives, BLDC drives, PMSM drives, LIM drives, propulsion technology for vehicles, measurement techniques, open-end winding drives, driver circuits, and digital control.